Faraday Discussions

Trends in the Thermal Stability of Two-Dimensional Covalent Organic Frameworks

Journal:	*Faraday Discussions*
Manuscript ID	FD-ART-05-2020-000054.R1
Article Type:	Paper
Date Submitted by the Author:	19-Jun-2020
Complete List of Authors:	Evans, Austin; Northwestern University, Chemistry Ryder, Matthew; Oak Ridge National Laboratory, Neutron Scattering Division Ji, Woojung; Northwestern University, Chemistry Strauss, Michael; Northwestern University, Chemistry Corcos, Amanda; Northwestern University, Chemistry Vitaku, Edon; Northwestern University, Department of Chemistry Flanders, Nathan; Northwestern University, Chemistry Bisbey, Ryan; Northwestern University, Chemistry Dichtel, William; Northwestern University, Chemistry

Paper

Trends in the Thermal Stability of Two-Dimensional Covalent Organic Frameworks

Austin M. Evans,[1] Matthew R. Ryder,[2] Woojung Ji,[1] Michael J. Strauss,[1] Amanda R. Corcos,[1] Edon Vitaku,[1] Nathan C. Flanders,[1] Ryan P. Bisbey,[1] and William R. Dichtel*,[1]

Two-dimensional covalent organic frameworks (2D COFs) are synthetically diverse, layered macromolecules. Their covalent lattices are thought to confer high thermal stability, which is typically evaluated with thermogravimetric analysis (TGA). However, TGA measures the temperature at which volatile degradation products are formed and is insensitive to changes of the periodic structure of the COF. Here, we study the thermal stability of ten 2D COFs using a combination of variable-temperature X-ray diffraction, TGA, diffuse reflectance infrared spectroscopy, and density-functional theory calculations. We find that 2D COFs undergo a general two-step thermal degradation process. At a first degradation temperture, 2D COFs lose their crystallinity without chemical degradation. Then, at higher temperatures, they chemically degrade into volatile byproducts. Several trends emerge from this exploration of 2D COF stability. Boronate ester-linked COFs are generally more thermally stable than comparable imine-linked COFs. Smaller crystalline lattices are more robust to thermal degradation than chemically similar, larger lattices. Finally, pore-functionalized COFs degrade at significantly lower temperatures than their unfunctionalized analogues. These trends offer design criteria for thermally resilient 2D COF materials. These findings will inform and encourage a broader exploration of mechanical deformation in 2D networks, providing a necessary step towards their practical use.

Received 00th January 20xx,
Accepted 00th January 20xx
DOI: 10.1039/x0xx00000x

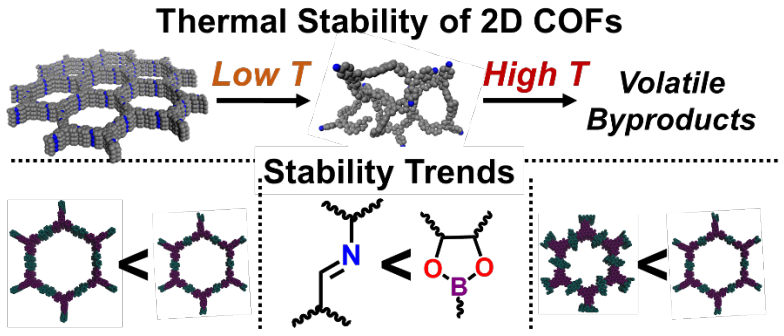

TOC Graphic

[1]Northwestern University, Department of Chemistry, 2145 Sheridan Road, Evanston, IL 60208, USA
E-mail:wdichtel@northwestern.edu
[2]Neutron Scattering Division, Oak Ridge National Laboratory, Oak Ridge, TN, 37831, USA
† Electronic supplementary information (ESI) available. See DOI:

Introduction

Two-dimensional covalent organic frameworks (2D COFs) are a maturing class of modular, structurally regular, permanently porous, layered polymers. This unique combination of properties has inspired interest in several applications, many of which will require highly stable materials.[1, 2] Since the earliest reports of 2D COF synthesis, researchers have speculated that their strong and structurally regular covalent bonds would make them robust to chemical, thermal, and mechanical stress.[3, 4] Thermogravimetric analysis (TGA) performed in many 2D COF reports supported this view, in that temperatures as high as 800 °C are required to release volatile degradation byproducts.[3] Their desirable thermal stability has been noted as an important design criterion as COFs have been explored for applications such as sensing,[5-8] catalysis,[9, 10] optoelectronics,[6, 11-13] energy storage,[11, 14] and chemical separations,[7, 15-17] which sometimes operate under demanding thermomechanical stresses.

We recently compared the thermal stability of a pair of structurally similar but chemically distinct 2D COFs[18] using TGA and variable-temperature X-ray diffraction (VT-XRD, **Figure 1A**). Both COFs exhibited two degradation temperatures: a lower temperature at which the materials lose their periodicity (T_{XRD}) but retain their chemical structure, and a higher temperature (T_{TGA}) at which chemical degradation generates volatile byproducts (**Figure 1B**). VT-XRD and density functional theory (DFT) revealed evidence for buckling of these two COF lattices as they approach T_{XRD}, further suggesting that the COFs lose crystallographic registry through structural distortions prior to covalent depolymerization. These observations indicate that the structural regularity of COFs, which distinguishes them from conventional cross-linked polymer networks, is less thermally robust than is captured by TGA.

Recent indirect experimental evidence also supports the hypothesis that 2D COF layers are susceptible to structural deformation during isolation or characterization. For example, Bunck *et al.* found that

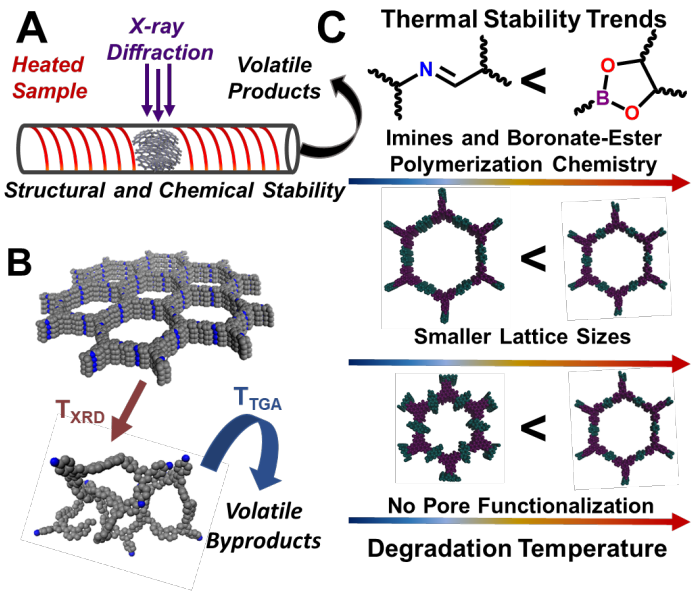

Fig. 1 (A) Schematic illustration of variable-temperature measurements. (B) Schematic illustration of two different degradation processes studied in this work. (C) 2D COF Thermal stability trends observed in this work.

hydrazone-linked networks spontaneously exfoliate when immersed in common organic solvents, which was attributed to the weak interlayer interactions of hydrazone-linked 2D COFs.[19] More recently, studies conducted by Sick *et al.* and Feriante *et al.* observed that many imine-linked 2D COFs became amorphous and lose porosity when exposed to vacuum.[20, 21] Gole *et al.* and Li *et al.* found that even with the nanoscale COF net preserved, mesoscale mechanical deformation of 2D layers is energetically feasible.[7, 22] These findings are consistent with earlier theoretical work on the mechanics of 2D polymers, which found their deformation is driven by entropic forces, similar to disorder in linear polymer networks.[23-26] These observations motivate a thorough investigation into the mechanics of covalent 2D networks, which have yet to be systematically explored. A deeper investigation into the thermomechanical deformations of layered crystalline polymers will be invaluable in developing the most promising applications of 2D COFs.

Herein, we characterize the thermal stability of ten 2D COFs and find that in all cases, the periodic COF structure deforms at lower temperatures than the degradation temperature assessed by TGA. Based on VT-XRD, TGA, diffuse reflectance infrared spectroscopy (DRIFTS), and DFT calculations, we conclude that all COFs become disordered without significant chemical degradation at a temperature (T_{XRD}) lower than their T_{TGA} (**Figure 1A and 1B**). Several trends emerge from studying this process across many 2D COFs (**Figure 1C**). Boronate ester-linked materials are more stable than structurally similar imine-linked frameworks. Smaller lattices are more thermally stable than their larger analogues. Finally, the T_{XRD} of 2D COFs decreases in networks with functional groups in their pores, despite these groups not significantly impacting T_{TGA}. To more accurately assess the thermal stability of 2D polymers, structural analysis, including N_2 sorption measurements, XRD, or direct imaging should be used in conjunction with TGA. Furthermore, these results show that the fabrication or measurement of devices based on 2D COFs should be carefully considered, as processing techniques and temperatures, in some cases, are not benign. Overall, the structural trends for retaining crystallinity to relatively high temperatures suggest various strategies to control thermal stability through judicious design.

Results and Discussion

Synthesis and Characterization of COF Powders

To study their thermal stability, we prepared high-quality 2D COF powders via previously reported methods (**Scheme S1 - S21**).[3, 17, 27-30] In all cases, room temperature XRD showed narrow 100 Bragg peaks and several higher-order diffraction features. By considering finite crystallite size broadening of the XRD patterns with full pattern Le Bail fitting, we ascertained that the crystallite domain sizes are on the order of 50–100 nm, consistent with reports of high-quality COFs in the literature (**Figure S12 – S55**).[28] Similarly, Brunauer-Emmett-Teller (BET) N_2 surface areas revealed experimental surfaces areas close to each COF's respective theoretical Connolly surface area and narrow pore width distributions consistent with Pawley refined structures (**Figure S56 – S77**). Fourier-transform infrared (FT-IR) spectroscopy revealed near-complete polymerization conversion by the disappearance of monomer IR features and the emergence of the expected polymer IR features in their respective IR spectra (**Figure S78 – S88**).

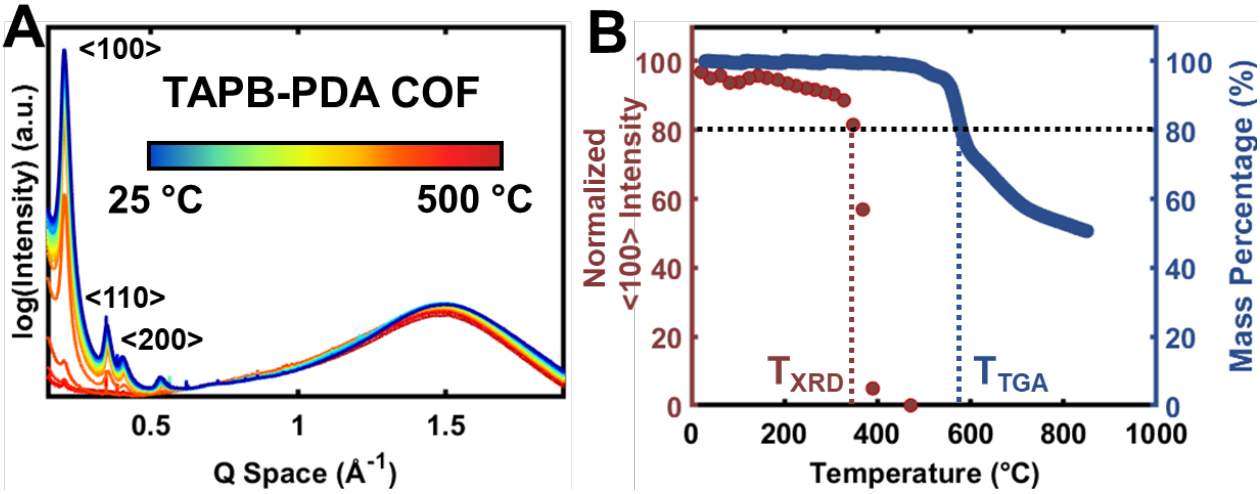

Fig. 2 (A) Variable-temperature X-ray diffraction of TAPB-PDA COF. (B) Comparison of the 100 diffraction intensity and sample mass as a function of temperature.

Taken together, these experiments indicate that the materials used in this study are of similar or higher quality than those evaluated in leading literature reports.

Amorphization and Volatilization: Two Degradation Temperatures

VT-XRD reveals that T_{XRD} is lower than T_{TGA} for all 2D COFs investigated. As an example, we studied the thermal stability of the prototypical imine-linked 2D COF, TAPB-PDA, which is formed by condensing 1,3,5-tris(aminophenyl)benzene (TAPB) and 1,4-phenylenedialdehyde (PDA, **Scheme S13 and Figure S3**). The COF powder was heated at 10 °C min^{-1} under an inert atmosphere while continuously monitoring either the mass or synchrotron diffraction pattern (**Figure 2A**). We define the structural deformation temperature as either when the integrated 100 Bragg diffraction feature (T_{XRD}) or the mass of the sample (T_{TGA}) dropped below 80% of their room-temperature values (**Figure 2B**).[12] TAPB-PDA thermally decomposes at 550 °C (T_{TGA}) (**Figure 2B**), which agrees with T_{TGA} reported for TAPB-PDA and other imine-linked frameworks in previous reports.[31-33] However, TAPB-PDA loses crystallinity at 320 °C (**Figure 2B**). This large difference (230 °C) highlights that the thermal degradation temperature assessed by TGA is not representative of COF structural stability. Additionally, the observation of two degradation temperatures, one related to the loss of crystallinity and another related to volatilization of the network, demonstrates that 2D COFs form an intermediate disordered phase that subsequently degrades to volatile species at higher temperatures.

Comparisons of COF Stability and Structural Trends

The presence of two distinct degradation temperatures is general for all COFs that were studied, with boronate ester-linked networks with smaller lattices found to be more thermally stable than their larger analogues. This trend is evident by comparing the thermal stability of two hexagonal boronate ester-linked 2D COF frameworks, HHTP-PBBA (previously reported as COF-5)[3] and HHTP-BBBA (previously reported as COF-10),[27] which are synthesized by the condensation of 2,3,6,7,10,11-hexahydroxytriphenylene (HHTP) and 1,4-phenylenebis(-boronic acid) (PBBA) or

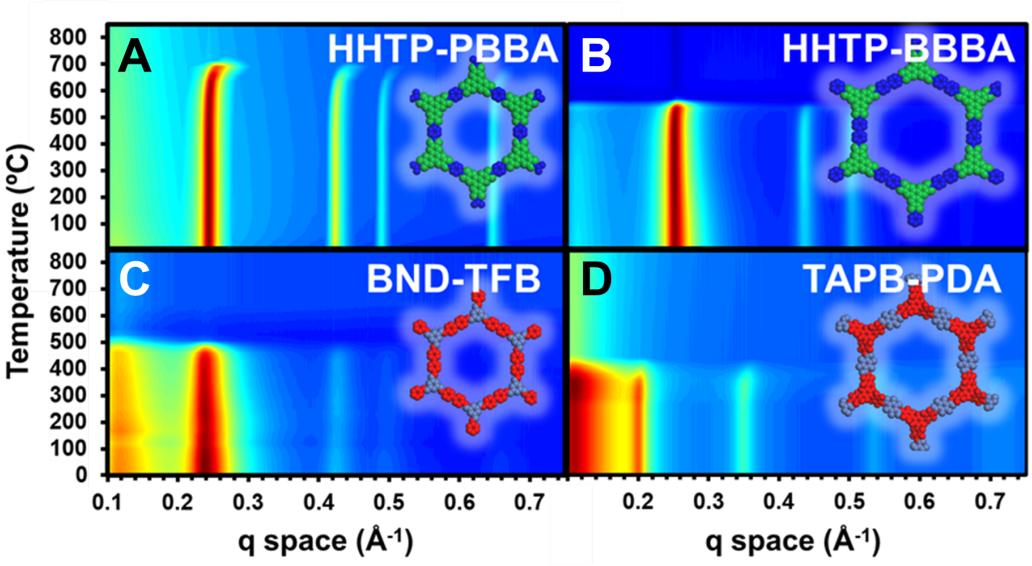

Fig. 3. Variable-temperature X-ray scattering profiles of four commonly studied COFs: the boronate ester-linked **A)** HHTP-PBBA COF and **B)** HHTP-BBBA COF, and the imine-linked **C)** BND-TFB COF and **D)** TAPB-PDA COF.

4,4'-biphenylbis(boronic acid) (BBBA), respectively (**Scheme S11 and S12, and Figure S1 and S2**). These hexagonal networks are chemically similar but differ primarily in their lattice sizes: HHTP-PBBA has an in-plane lattice size of 28 Å, and HHTP-BBBA has an in-plane lattice size of 34 Å. TGA revealed a primary mass loss event at T_{TGA} = 750 °C for HHTP-PBBA (**Figure S97**) and T_{TGA}= 500 °C for HHTP-BBBA (**Figure S98**), which are consistent with previous reports.[3, 4] However, HHTP-PBBA and HHTP-BBBA lose their crystallographic registry at T_{XRD} = 600 °C and T_{XRD} = 400 °C, respectively (**Figure 3A and 3B**). While boronate ester-linked COF's structures are stable to high temperatures, much like their imine-linked counterparts, they form a disordered phase prior to degrading to volatile by-products. Furthermore, because both T_{TGA} and T_{XRD} decrease in COFs with larger lattice sizes suggests that both the chemical and structural degradation mechanisms are related to the size of the crystalline COF lattice. This trend is also observed for imine-linked 2D COFs. We investigated two imine-linked- 2D COFs, TAPB-PDA (**Figure S3 and Scheme S13**) and BND-TFB (**Figure S10 and Scheme S20**), which are synthesized by the condensation of tris(4-aminophenyl)benzene (TAPB) and 1,4-phenyldialdehyde (PDA) and *N*-benzidine benzophenone imine (BND) and 1,3,5-triformylbenzene (TFB), respectively. Both COFs exhibit a T_{TGA} of 550°C (**Figure S99 and Figure S106**).[31-33] Both imine-linked networks have lower T_{XRD}, with T_{XRD} = 365 °C for BND-TFB (**Figure 3C**) and T_{XRD} = 320 °C for TAPB-PDA (**Figure 3D**). In this case, the smaller BND-TFB (28 Å) is 45 °C more stable than TAPB-PDA (32 Å). Ostensibly, the lower stability of larger 2D networks is due to their larger free volumes, a higher number of deformation points (rotatable bonds) per unit cell, and additional accessible phonon modes. We suspect that a complex interplay of factors could lead to this observed trend in degradation temperature. These factors are all compatible with the understanding that structural distortions in 2D layers are entropically driven. As a consequence of this trend, it is likely is a trade-off between increased pore size and decreased thermal stability.

By comparing chemically distinct COFs with similar lattice sizes and symmetries, COFs polymerized through boronate esters are observed to be more thermally stable than their imine-linked counterparts. Pawley refined crystal structures reveal that the imine-linked BND-TFB (28 Å) and boronate ester-linked HHTP-PBBA (29 Å) and the imine-linked TAPB-PDA (32 Å) and boronate ester-linked HHTP-BBBA (34 Å) are of similar unit cell sizes. In both

cases, the boronate ester-linked frameworks are >100 °C more stable than imine-linked frameworks as judged by T_{XRD}. The increased thermal stability of boronate ester-linked frameworks may be related to the larger van der Waals surfaces of these HHTP-containing structures or may be more generally related to the increased structural rigidity of boronate-esters compared to those of imines.[34] These comparisons highlight an important consideration when selecting polymerization chemistries to be tailored for intended use of the COF. For example, boronate ester-linked frameworks are less hydrolytically stable than imine-linked frameworks, yet they may be preferable in anhydrous environments and applications wherein high thermal stabilities are desired.

Thermally Driven Buckling of Boronate Ester-Linked 2D COFs

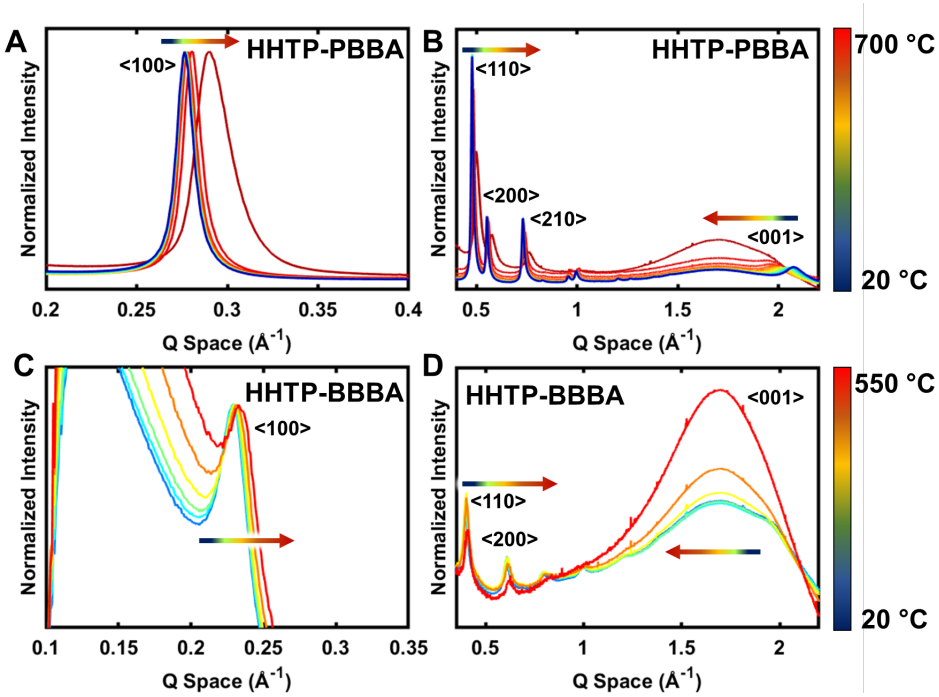

Fig. 4. Normalized temperature-dependent X-ray diffraction profiles of **(A)** HHTP-PBBA small-angle scattering **(B**) HHTP-PBBA wide angle scattering **(C)** HHTP-BBBA small-angle scattering and **(D)** HHTP-BBBA wide angle scattering.

As boronate ester-linked frameworks approach T_{XRD}, their in-plane lattices contract, which provides insight into the mechanism of their transient amorphization. As both PBBA-HHTP and BBBA-HHTP were heated to their T_{XRD}, their in-plane Bragg diffraction features (100 (**Figure 4A**), 110, 200, 210 (**Figure 4C**) trended towards higher values in reciprocal space. The maximum diffraction feature trending towards higher values in reciprocal space corresponds to the in-plane crystallographic direction undergoing the unusual process of thermal contraction. In contrast, heating both COFs led to the maximum cross-plane diffraction features (001) shifting to lower reciprocal space (**Figure 4B and 4D**), indicating thermal expansion. Recently, we proposed that these changes represented a phase change wherein 2D layers buckle with respect to each other, thereby shrinking the in-plane crystallographic direction.[35] The structural changes observed here for boronate ester-linked COFs support this hypothesis. Therefore, we suspect that amorphization is unlikely to correspond to chemical degradation of the network and is instead structural in nature, consistent with similar findings related to metal-organic frameworks.[36] Likely, a large amount of softening and expansion as a function of temperature for boronate ester-linked COFs is related to the

high temperatures accessible by their thermally stable structures, large pore volumes, and a large number of accessible phonon modes in all-organic frameworks. These observations of dynamic COF structures may inspire their use when responsive, highly stable crystalline lattices are desirable.

In contrast to the behavior of the boronate ester-linked COFs, the imine-linked TAPB-PDA COF does not undergo the same degree of thermal contraction as it approaches its T_{XRD}. In TAPB-PDA and its structural analogues (**Figure 5A**), the diffraction features do not shift appreciably during heating (**Figure 2A** and **Figure 5B**). We suspect that the origin of this difference is the inherent distortions associated with TAPB-PDA. In boronate ester-linked frameworks, COF layers exhibit minimal out-of-plane distortions as a result of their highly planar monomers and the rigidity of boronate-ester bonds. In contrast, TAPB-PDA layers are considerably rotated (**Figure S107**), which primarily from the steric strain of the tris(phenyl)benzene moiety. DFT calculations suggest that this rotational freedom allows for the relaxation of thermally induced stress without significant buckling of the 2D COF layers (**Figure S108**). This observation demonstrates that there are opportunities to prevent thermal contraction in 2D COFs. Taken together, these pairwise comparisons will guide the future design of 2D COFs with high stabilities and/or dynamic mechanical properties.

Thermal Stability of 2D COFs with Functionalized Pores

Chemically modifying the pores of a COF containing reactive pendant groups, sometimes known as pore-surface functionalization, is a powerful strategy to generate a diverse set of 2D COFs from a single precursor framework. This approach has been used to tailor COFs of interest for organic electronic devices, adsorbents, and membranes.[17, 29, 37] However, it is not known how side chains impact the thermal stability of the 2D COFs. We synthesized microcrystalline powders of functionalized TAPB-PDA-R COFs, where R = H, Me, Et, Br, SMe, by the condensation of TAPB and the corresponding 2,5-disubstituted terephthaldehyde (PDA-R) (**Figure 5A, Scheme S16 – S19**). In all cases, the T_{TGA} of these networks was similar to the parent TAPB-PDA (all approximately 500 °C, **Figure S102 - 105**). This finding suggests that bond breaking and subsequent volatilization likely originates along the parent framework backbone, not the side chains.

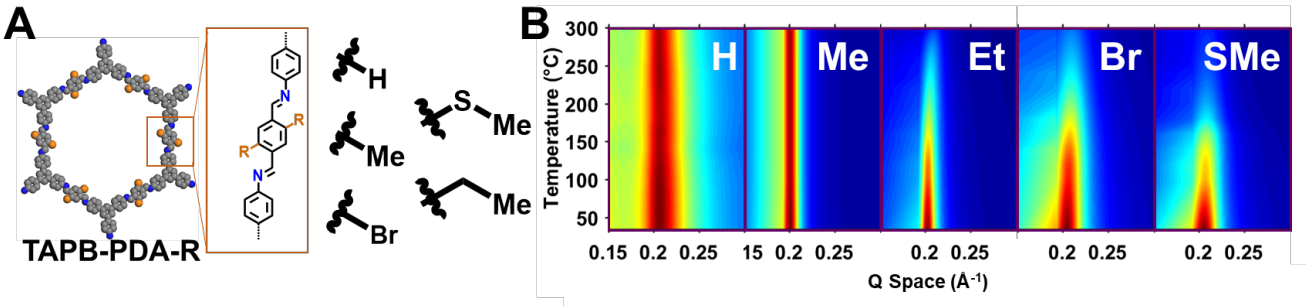

Fig. 5. (A) Structures of pore-functionalized TAPB-PDA-R COFs. **(B)** VT-XRD of TAPB-PDA-R.

Despite their similar T_{TGA} values, the T_{XRD} of these networks varied greatly. The T_{XRD}s of the R= H, Me, Et, Br, SMe networks were >300°C, >300°C, 250°C, 150°C, and 125°C, respectively (**Figure 5B**). Taken together, this trend shows that as larger substituents are added to the pore surface, the temperature at which crystallinity is lost decreases. The reduced thermal stability of pore-functionalized networks may be related to the larger number of entropic states available to these networks, similar to entropic structural distortions in linear polymer systems,[38] or steric repulsion of the added functionalization in the pore. Both may cause significant disruption of interlayer interactions in 2D COF sheets, where larger, more mobile side chains act to force the layers apart as thermal energy is added to the system.

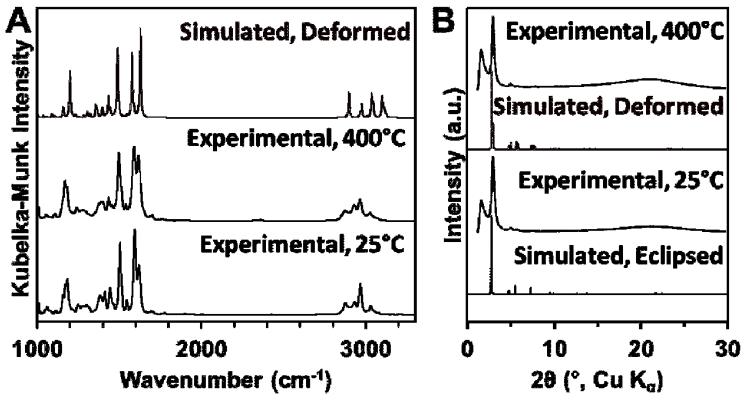

Fig. 6. (A) Comparison of variable-temperature diffuse reflectance infrared spectra and calculated infrared spectra of TAPB-PDA-Et COF **(B)** Comparison of experimental variable-temperature X-ray diffraction patterns and simulated X-ray diffraction from DFT optimized eclipsed and deformed phases of TAPB-PDA-Et COF.

DRIFTS and DFT calculations suggest that the origin of the thermally induced disorder is the disrupted registry of COF layers. Consistent with the TGA, we find that most FT-IR features in TAPB-PDA-Me and TAPB-PDA-Et remain unchanged as the sample was heated to 500 °C (**Figure 6A and Figure S89 – S96**). Specifically, we find that the imine-feature remains intact across the entirety of the thermal ramp in both materials, indicating that substantial hydrolysis or transimination does not occur as a function of temperature. The high wavenumber FT-IR features (2500 – 3300 cm^{-1}) shifted slightly in location and relative intensity as the sample was heated, which could be due to the increased flexibility of their methyl and ethyl groups, respectively (**Figure 6A and Figure S89 – S96**). This observation is consistent with the hypothesis that the side chains cause structural distortions rather than chemical degradation. These experimental observations are consistent with computational results that show that the structures are unlikely to buckle or deform as significantly to previous studies on 2D COFs.[35] The DFT calculated IR spectrum from a relaxed structure is in strong agreement with experiment (**Figure 6A and Figure S111 – S113**). Similarly, simulated diffraction patterns from a DFT calculated deformed structure and perfectly eclipsed structure show that only minor structural differences arise as the TAPB-PDA-Et COF deforms, consistent with our experimental observations (**Figure 6B**). Taken together, the effects of pore functionalization are reminiscent of plasticization of 1D polymers and intercalation-driven exfoliation of 2D materials. As such, we suspect that pore functionalization may be a versatile platform to control thermomechanical processes in 2D polymers.

Chemically Reactive Pore Functionalization

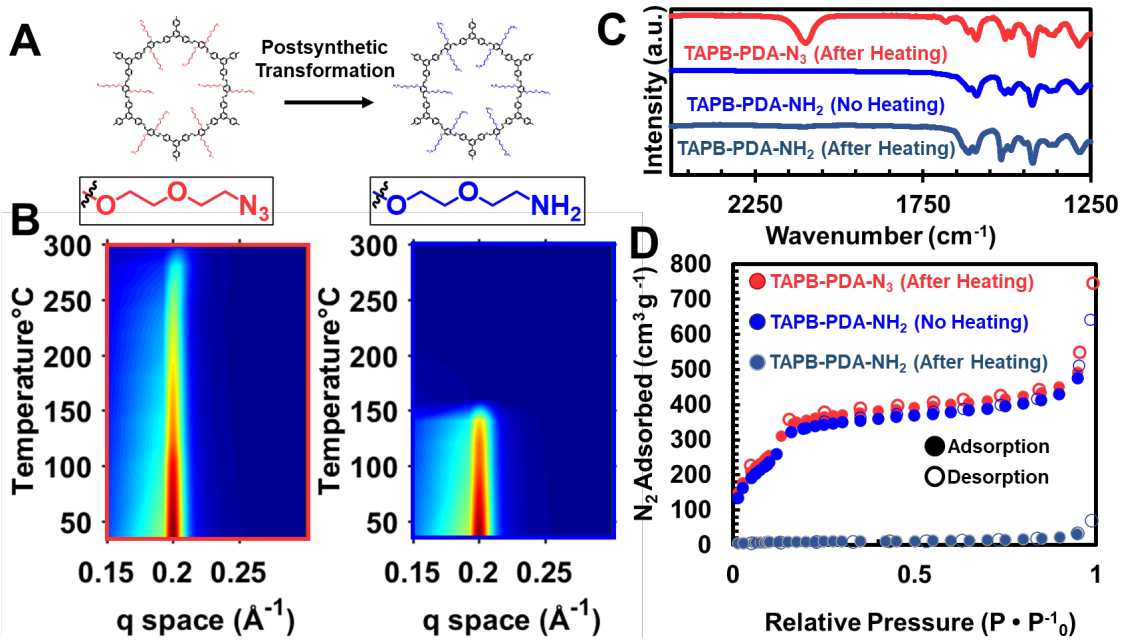

Fig. 7. (A) Chemical structures of the TAPB-PDA-N_3 and TAPB-PDA-NH_2 COFs **(B)** VT-XRD of TAPB-PDA-N_3 and TAPB-PDA-NH_2 COF. **(C)** IR spectra of TAPB-PDA-N_3 and TAPB-PDA-NH_2 COF after heating and TAPB-PDA-NH_2 COF without heating. **(D)** N_2 isotherms of TAPB-PDA-N_3 and TAPB-PDA-NH_2 COF after heating and TAPB-PDA-NH_2 COF without heating.

In addition to structural distortions induced by smaller side chains, chemically active side chains also degrade the COF structure during thermal activation. To investigate the role of such side chains, we first synthesized TAPB-PDA-N_3, by condensing TAPB and a PDA with an azide-functionalized glycol chain (**Figure 7A**). The azides were reduced to amines to produce TAPB-PDA-NH_2 in quantitative yield. Despite being nearly identical in size, the amine-functionalized network (T_{XRD} = 120 °C) degrades 50 °C lower than its azide-functionalized counterpart (T_{XRD} = 170 °C) (**Figure 7B**). The amine-functionalized framework had unique transient diffraction features that appeared before its amorphization (**Figure 7B**), which led us to speculate that the amines were reacting in the solid-state by nucleophilic addition to the imine linkages of the COF. This process is feasible in the monomer; upon reduction of PDA-N_3 to PDA-NH_2, an intramolecular condensation with its aldehydes occurs in high yields (>70%), which prevented its direct polymerization into a COF (**Figure S114 and S115**). The low temperature of amorphization for TAPB-PDA-NH_2 allowed us to study the degradation of this network using N_2 porosimetry. Before N_2 sorption isotherm measurements, samples are frequently heated to remove volatile solvents. However, when TAPB-PDA-NH_2 was degassed at 100 °C for 15 hours, it became amorphous and nonporous (**Figure 7D**). In contrast, TAPB-PDA-N_3 survived degassing at 100 °C for 15 hours with retention of its high surface area. However, when degassed at room temperature TAPB-PDA-NH_2 retained its high surface area suggesting that even mild heating drove amorphization in this network. FT-IR measurements performed before and after degassing of TAPB-PDA-NH_2 COF shows limited changes, both of which are similar to the parent TAPB-PDA COF and TAPB-PDA-N_3 COF, which does not preclude that substantial transimination has occurred (**Figure 7C**). Taken together, these results suggest that solid-state reactions can occur under thermal stresses when incompatible chemistries are present in the same

framework. However, it also points to a more exciting possibility that COFs with designed, thermally switchable depolymerization processes might be realized by controlled functional group manipulations.

Conclusions

COFs are an emerging class of crystalline, permanently porous, polymers with proposed applications ranging from catalyst supports to energy storage materials. Due to their covalently bonded network structures, these materials are thought to be highly stable. TGA experiments have historically supported this view. Variable-temperature X-ray diffraction experiments demonstrate that the thermal degradation processes of 2D COFs are more complex. In the ten COFs studied here, amorphization occurs well before degradation is detected by TGA. These experiments suggest several trends between chemical structure and stability. First, boronate ester-linked 2D COFs are more stable than their imine-linked counterparts. Second, smaller networks were more thermally stable than their larger analogues. Finally, pore functionalization reduces the thermal stability of the periodic COF structure, in some cases by hundreds of degrees Celsius. A combination of experimental X-ray diffraction experiments and DFT calculations suggest that this amorphization process arises from structural deformation of COF layers, not substantial bond breakage. These findings suggest that the thermal stability of 2D COFs can be designed rationally by considering these fundamental trends and developing new strategies to tune the mechanics of 2D networks, such as reinforcing layers with secondary non-covalent interactions.[39]

Furthermore, these results should encourage a broader re-evaluation of 2D COF stability. Several instances of COFs being damaged by benign conditions, such as vacuum and mild heating, have now been reported. We suspect that in many cases, COF syntheses may be deemed unsuccessful due to their thermomechanical instability rather than polymerization failure. Moreover, seemingly innocuous isolation, property measurements, or device integration processes may damage the COF structure more is commonly appreciated. Therefore, it is essential that COFs with emergent properties be structurally characterized in their application-relevant forms (i.e., films, membranes, colloids), ideally both before and after the property of interest is measured. This guideline is even more important when measuring phenomena likely to be sensitive to the regular structure of 2D COFs, including electronic, optical, or magnetic properties. We also hope that this understanding will encourage further investigations into the origin of the amorphization, the intermediate disordered phase, and methods to control thermal stability. These insights will enable future 2D COFs to exhibit useful emergent properties that leverage their precise and designable molecular architectures, while achieving sufficient stability for applications.

Experimental

Thermogravimetric Analysis. Thermogravimetric analysis (TGA) was performed on a Netzch Simultaneous Thermal Analysis (STA) system using approximately 5 mg of sample. The samples were at a rate of 10 ˚C min^{-1} under a helium atmosphere until the mass degraded below 50% of its initial value or until it reached a temperature of 850 ˚C.

Variable-Temperature X-ray Diffraction. *In operando* X-ray diffraction was performed at Sector 17 and Sector 5 of the Advanced Photon Source (APS), Argonne National Laboratory. Samples were prepared by packing ~25 mg of COF sample into a thick-walled capillary and mounted into a heated sample stage. A thermocouple was then mounted in the center of the powder sample, inside of the capillary. The sample was then placed under a constant stream of inert gas and heated at a rate of 10 ˚C min^{-1}. Diffraction patterns were collected continuously throughout the heating cycle on a 2D Pilatus detector. These frames were then radially integrated to produce 1D diffraction

patterns by proprietary software available at the beamline, which were then analyzed. The data as shown were normalized by dividing all values by the scattering intensity of the initial (room temperature) 100 scattering feature.

Nitrogen Sorption Experiments. Gas adsorption isotherms were conducted on a Micromeritics Accelerated Surface Area and Porosity (ASAP) 2420 Analyzer. Typically, 20-50 mg samples were transferred to dried and tared analysis tubes equipped with filler rods and capped with a Transeal. The samples were heated to 40 °C at a rate of 1 °C/min and evacuated at 40 °C for 20 min, then heated to 100 °C at a rate of 1 °C/min heat, and evacuated at 100 °C until the outgassing rate was ≤0.3 μmHg/min (holding the samples at 100 °C for 5 hours was sufficient). At that point, the tube was weighed again to determine the mass of the activated sample. The tube was then transferred to the analysis port of the instrument. Ultra-high-purity-grade (99.999% purity) N_2 was used for all adsorption measurements. N_2 isotherms were generated by incremental exposure up to 760 mmHg (1 atm) in a liquid nitrogen (77 K) bath. Oil-free vacuum pumps and oil-free pressure regulators were used for all measurements. Brunauer-Emmett-Teller (BET) surface areas were calculated from the linear region of the N_2 isotherm at 77 K within the pressure range P/P_0 of 0.05–0.10.

Diffuse-Reflectance Infrared Spectroscopy. DRIFTS experiments were conducted on a Thermo-Fisher 6700 infrared (IR) spectrometer with a Harrick Praying Mantis attachment. Powder samples were loaded into the attachment with a KBr carrier to reduce the optical density of the COF powders. These samples were then heated at 10 ˚C min^{-1} under a constant argon flow with continuous monitoring of the IR spectra.

Diffraction Modeling. The crystal structures of the COFs were modeled using the Materials Studio (ver.5.0) suite of programs by Accelrys. The initial structures were constructed piecewise, starting with a primitive hexagonal unit cell with space group *P6*. The *a* unit cell parameter was estimated according to the distance between the center of the vertices for each COF, and *c* parameter was arbitrarily chosen as 3.35 Å. The structures and unit cell parameters were then optimized using the Forcite module and Universal Force Field. Calculation of the simulated powder diffraction patterns and Pawley refinements were performed using the Materials Studio Reflex Plus Module using a Bragg-Brentano geometry. The observed diffraction patterns were subjected to polynomial background subtraction and then to Pawley refinement, where the peak profile was refined using the Pseudo-Voigt peak shape function, and asymmetry was corrected using the Berar-Baldinozzi function. Crystallite size was estimated by the Le Bail method, which was refined to the experimental data. Surface area calculations were carried out using a Connolly surface calculation using the appropriate parameters for nitrogen as the adsorbed gas.

Density Functional Theory Calculations. DFT calculations were performed using the periodic *ab initio* code CRYSTAL17.[40] The PBE exchange-correlation functional[41] was used with a semi-empirical dispersion correction (PBE-D3)[42] to better account for the noncovalent interactions present in the 2D COF structures. The calculations were performed with all-electron atom-centered Gaussian-type basis sets of triple-zeta quality, previously shown to provide accurate structural and vibrational properties of flexible porous materials.[43, 44] The lattice parameters and atomic coordinates were optimized while initially maintaining the space group symmetry (*P6*) and then scanning the resultant vibrational modes and reducing the symmetry (*P1*) to investigate the deformed geometry. The IR intensities were computed using the Berry Phase approach.[45]

Conflicts of Interest

The authors declare no conflicts of interest.

Disclaimer

Acknowledgements

This work was supported by the National Science Foundation (NSF) through the Northwestern Materials Research Science and Engineering Center, under NSF Award DMR-1720139 and by the Army Research Office, under the Multidisciplinary University Research Initiative (MURI) program, Award W911NF-15-1-0447, and under Grant W911NF-17-1-0339. A.M.E (DGE-1324585) and M.J.S. (DGE-1842165) are supported by the NSF Graduate Research Fellowship and the International Institute for Nanotechnology through the Ryan Fellowship. Parts of this work were performed at the DuPont−Northwestern−Dow Collaborative Access Team (DND-CAT) located at Sector 5 of the Advanced Photon Source (APS). DND-CAT is supported by Northwestern University, E.I. DuPont de Nemours & Co., and the Dow Chemical Company. This research used resources of the Advanced Photon Source (Sector 5 and Sector 17) and Center for Nanoscale Materials, both U.S. Department of Energy (DOE) Office of Science User Facilities operated for the DOE Office of Science by Argonne National Laboratory under Contract DE-AC0206CH11357. This work has made use of the IMSERC facility, which has received support from the Soft and Hybrid Nanotechnology Experimental (SHyNE) Resource (NSF NNCI-1542205), the State of Illinois, and International Institute for Nanotechnology (IIN). This study also made use of the EPIC facility of NUANCE Center at Northwestern University, which has received support from the Soft and Hybrid Nanotechnology Experimental (SHyNE) Resource (NSF ECCS-1542205), the MRSEC program (NSF DMR-1720139) at the Materials Research Center, the Keck Foundation, the State of Illinois, and International Institute for Nanotechnology (IIN). M.R.R. acknowledges the U.S. Department of Energy (DOE) Office of Science (Basic Energy Sciences) for research funding and the National Energy Research Scientific Computing Center (NERSC), a U.S. Department of Energy (DOE) Office of Science User Facility, operated under Contract No. DE-AC02- 05CH11231, for access to supercomputing resources. We thank Rebecca Li for helpful discussions.

Notes and References

1. S.-Y. Ding and W. J. C. S. R. Wang, *Chem. Soc. Rev.*, 2013, **42**, 548-568.
2. X. Feng, X. Ding and D. J. C. S. R. Jiang, *Chem. Soc. Rev.*, 2012, **41**, 6010-6022.
3. A. P. Cote, A. I. Benin, N. W. Ockwig, M. O'Keeffe, A. J. Matzger and O. M. Yaghi, *Science*, 2005, **310**, 1166-1170.
4. H. M. El-Kaderi, J. R. Hunt, J. L. Mendoza-Cortés, A. P. Côté, R. E. Taylor, M. O'Keeffe and O. M. Yaghi, *Science*, 2007, **316**, 268-272.
5. S. Jhulki, A. M. Evans, X.-L. Hao, M. W. Cooper, C. H. Feriante, J. Leisen, H. Li, D. Lam, M. C. Hersam, S. Barlow, W. R. Dichtel and S. R. Marder, *J. Am. Chem. Soc.*, 2020.
6. R. Kulkarni, Y. Noda, D. K. Barange, Y. S. Kochergin, P. Lyu, B. Balcarova, P. Nachtigall and M. J. Bojdys, *Nat. Comm.*, 2019, **10**, 1-8.
7. H. Li and J.-L. Brédas, *Chem. Mater.*, 2019, **31**, 3265-3273.
8. X. Wu, X. Han, Q. Xu, Y. Liu, C. Yuan, S. Yang, Y. Liu, J. Jiang and Y. Cui, *J. Am. Chem. Soc.*, 2019, **141**, 7081-7089.
9. E. Jin, Z. Lan, Q. Jiang, K. Geng, G. Li, X. Wang and D. J. C. Jiang, *Chem.*, 2019, **5**, 1632-1647.
10. X. Wang, X. Han, J. Zhang, X. Wu, Y. Liu and Y. Cui, *J. Am. Chem. Soc.*, 2016, **138**, 12332-12335.
11. A. K. Mandal, J. Mahmood and J. B. J. C. Baek, *Chem. Nano. Mat.*, 2017, **3**, 373-391.

12. A. M. Evans, I. Castano, A. Brumberg, L. R. Parent, A. R. Corcos, R. L. Li, N. C. Flanders, D. J. Gosztola, N. C. Gianneschi, R. D. Schaller and W. R. Dichtel, *J. Am. Chem. Soc.*, 2019, **141**, 19728-19735.
13. T. Sick, A. G. Hufnagel, J. Kampmann, I. Kondofersky, M. Calik, J. M. Rotter, A. Evans, M. Döblinger, S. Herbert, K. Peters and T. Bein, *J. Am. Chem. Soc.*, 2017, **140**, 2085-2092.
14. C. R. DeBlase, K. E. Silberstein, T.-T. Truong, H. c. D. Abruña and W. R. Dichtel, *J. Am. Chem. Soc.*, 2013, **135**, 16821-16824.
15. H. Fan, M. Peng, I. Strauss, A. Mundstock, H. Meng and J. Caro, *J. Am. Chem. Soc.*, 2020.
16. S. Yuan, X. Li, J. Zhu, G. Zhang, P. Van Puyvelde and B. J. C. S. R. Van der Bruggen, *Chem. Soc. Rev.*, 2019, **48**, 2665-2681.
17. A. R. Corcos, G. A. Levato, Z. Jiang, A. M. Evans, A. G. Livingston, B. J. Mariñas and W. R. Dichtel, *ACS Mater. Lett.*, 2019, **1**, 440-446.
18. A. M. Evans, M. R. Ryder, N. C. Flanders, E. Vitaku, L. X. Chen and W. R. Dichtel, *Ind. Eng. Chem. Res.* , 2019, **58**, 9883-9887.
19. D. N. Bunck and W. R. Dichtel, *J. Am. Chem. Soc.*, 2013, **135**, 14952-14955.
20. C. H. Feriante, S. Jhulki, A. M. Evans, R. R. Dasari, K. Slicker, W. R. Dichtel and S. R. Marder, *Adv. Mater.*, 2019, 1905776.
21. T. Sick, J. M. Rotter, S. Reuter, S. Kandambeth, N. N. Bach, M. Döblinger, J. Merz, T. Clark, T. B. Marder and T. Bein, *J. Am. Chem. Soc.*, 2019, **141**, 12570-12581.
22. B. Gole, V. Stepanenko, S. Rager, M. Grüne, D. D. Medina, T. Bein, F. Würthner and F. Beuerle, *Angew. Chem. Int. Ed.*, 2018, **57**, 846-850.
23. J. L. Jacobsen and J. Kondev, *J. Stat. Phys.*, 1999, **96**, 21-48.
24. P. Payamyar, B. T. King, H. C. Öttinger and A. D. Schlüter, *Chem. Comm.*, 2016, **52**, 18-34.
25. E. Vernier, J. L. Jacobsen, H. J. J. o. S. M. T. Saleur and Experiment, *J. Stat. Mech.*, 2015, **2015**, P09001.
26. J. Nagle, *P. Roy. Soc. A-Math. Phy.*, 1974, **337**, 569-589.
27. C. J. Doonan, D. J. Tranchemontagne, T. G. Glover, J. R. Hunt and O. M. J. N. c. Yaghi, *Nat. Chem.*, 2010, **2**, 235-238.
28. M. C. Daugherty, E. Vitaku, R. L. Li, A. M. Evans, A. D. Chavez and W. R. Dichtel, *Chem. Comm.*, 2019, **55**, 2680-2683.
29. W. Ji, L. Xiao, Y. Ling, C. Ching, M. Matsumoto, R. P. Bisbey, D. E. Helbling and W. R. Dichtel, *J. Am. Chem. Soc.*, 2018, **140**, 12677-12681.
30. E. Vitaku and W. R. J. J. o. t. A. C. S. Dichtel, *J. Am. Chem. Soc.*, 2017, **139**, 12911-12914.
31. N. Mokhtari, M. M. Khataei, M. Dinari, B. H. Monjezi and Y. J. M. L. Yamini, *Mater. Lett.* , 2020, **263**, 127221.
32. M. G. Rabbani, A. K. Sekizkardes, Z. Kahveci, T. E. Reich, R. Ding and H. M. El-Kaderi, *Eur. J. Chem.*, 2013, **19**, 3324-3328.
33. F. J. Uribe-Romo, J. R. Hunt, H. Furukawa, C. Klock, M. O'Keeffe and O. M. J. J. o. t. A. C. S. Yaghi, *J. Am. Chem. Soc.*, 2009, **131**, 4570-4571.
34. Y.-R. Luo, *Comprehensive handbook of chemical bond energies*, CRC press, 2007.
35. D. W. Burke, C. Sun, I. Castano, N. C. Flanders, A. M. Evans, E. Vitaku, D. C. McLeod, R. H. Lambeth, L. X. Chen, N. C. Gianneschi and W. R. Dichtel, *Angew. Chem. Int. Ed.*, 2019.
36. A. J. Howarth, Y. Liu, P. Li, Z. Li, T. C. Wang, J. T. Hupp and O. K. J. N. R. M. Farha, *Nat. Rev. Mater.*, 2016, **1**, 1-15.
37. A. Nagai, Z. Guo, X. Feng, S. Jin, X. Chen, X. Ding and D. J. N. c. Jiang, *Nat. Comm.*, 2011, **2**, 1-8.
38. U. Gedde, *Polymer physics*, Springer Science & Business Media, 1995.
39. S. B. Alahakoon, G. T. McCandless, A. A. Karunathilake, C. M. Thompson and R. A. J. C. A. E. J. Smaldone, 2017, **23**, 4255-4259.
40. R. Dovesi, A. Erba, R. Orlando, C. M. Zicovich-Wilson, B. Civalleri, L. Maschio, M. Rerat, S. Casassa, J. Baima, S. Salustro and B. Kirtman, *Rev. Comput. Mol. Sci.*, 2018, **8**, e1360.
41. J. P. Perdew, K. Burke and M. Ernzerhof, *Phys. Rev. Lett.*, 1996, **77**, 3865-3868.
42. S. Grimme, J. Antony, S. Ehrlich and H. Krieg, *J. Chem. Phys.*, 2010, **132**, 154104.
43. M. R. Ryder, J. Maul, B. Civalleri and A. Erba, *Adv. Theory Simul.*, 2019, **2**, 1900093.
44. M. R. Ryder, B. Van de Voorde, B. Civalleri, T. D. Bennett, S. Mukhopadhyay, G. Cinque, F. Fernandez-Alonso, D. De Vos, S. Rudic and J. C. Tan, *Phys. Rev. Lett.*, 2017, **118**, 255502.
45. Y. Noel, C. M. Zicovich-Wilson, B. Civalleri, P. D'Arco and R. Dovesi, *Phys. Rev. B*, 2001, **65**.